Bulletin of the Seismological Society of America, Vol. 86, No. 1B, pp. S193–S208, February 1996

Directional Topographic Site Response at Tarzana Observed in Aftershocks of the 1994 Northridge, California, Earthquake: Implications for Mainshock Motions

by Paul Spudich, Margaret Hellweg, and W. H. K. Lee

Abstract The Northridge earthquake caused 1.78 *g* acceleration in the east–west direction at a site in Tarzana, California, located about 6 km south of the mainshock epicenter. The accelerograph was located atop a hill about 15-m high, 500-m long, and 130-m wide, striking about N78°E. During the aftershock sequence, a temporary array of 21 three-component geophones was deployed in six radial lines centered on the accelerograph, with an average sensor spacing of 35 m. Station C00 was located about 2 m from the accelerograph. We inverted aftershock spectra to obtain average relative site response at each station as a function of direction of ground motion. We identified a 3.2-Hz resonance that is a transverse oscillation of the hill (a directional topographic effect). The top/base amplification ratio at 3.2 Hz is about 4.5 for horizontal ground motions oriented approximately perpendicular to the long axis of the hill and about 2 for motions parallel to the hill. This resonance is seen most strongly within 50 m of C00. Other resonant frequencies were also observed. A strong lateral variation in attenuation, probably associated with a fault, caused substantially lower motion at frequencies above 6 Hz at the east end of the hill. There may be some additional scattered waves associated with the fault zone and seen at both the base and top of the hill, causing particle motions (not spectral ratios) at the top of the hill to be rotated about 20° away from the direction transverse to the hill. The resonant frequency, but not the amplitude, of our observed topographic resonance agrees well with theory, even for such a low hill. Comparisons of our observations with theoretical results indicate that the 3D shape of the hill and its internal structure are important factors affecting its response. The strong transverse resonance of the hill does not account for the large east–west mainshock motions. Assuming linear soil response, mainshock east–west motions at the Tarzana accelerograph were amplified by a factor of about 2 or less compared with sites at the base of the hill. Probable variations in surficial shear-wave velocity do not account for the observed differences among mainshock acceleration observed at Tarzana and at two different sites within 2 km of Tarzana.

Introduction

On the morning of 17 January 1994, the M_W 6.7 Northridge earthquake caused extremely violent shaking at a site in Tarzana, California, located about 6 km south and 18.7 km above the mainshock hypocenter (Fig. 1; Hauksson *et al.,* 1995). A Kinemetrics SMA-1 analog accelerograph operated at the Cedar Hill Nursery in Tarzana by the California Division of Mines and Geology (Shakal *et al.,* 1994) recorded an estimated peak horizontal acceleration of 1.78 *g* (phase 2, 1.93 *g* phase 1), one of the highest accelerations ever recorded in an earthquake. Two other accelerographs located within 2 km of the Cedar Hill Nursery recorded considerably smaller accelerations during the Northridge mainshock (Fig. 2). It is important to try to identify the factors that caused both the 1.78 *g* motion at the Cedar Hill Nursery and the differences between ground motions at these three sites so that these factors can be considered when making maps of expected shaking in future earthquakes.

Several authors (Shakal *et al.,* 1988; Vidale *et al.,* 1991) have identified an unusual seismic response of the Tarzana site during the 1987 Whittier Narrows mainshock and largest aftershock. The Tarzana site experienced the second largest peak acceleration in the Los Angeles region during the Whittier Narrows mainshock, despite being located 44 km from the epicenter. This peak acceleration was about a factor of

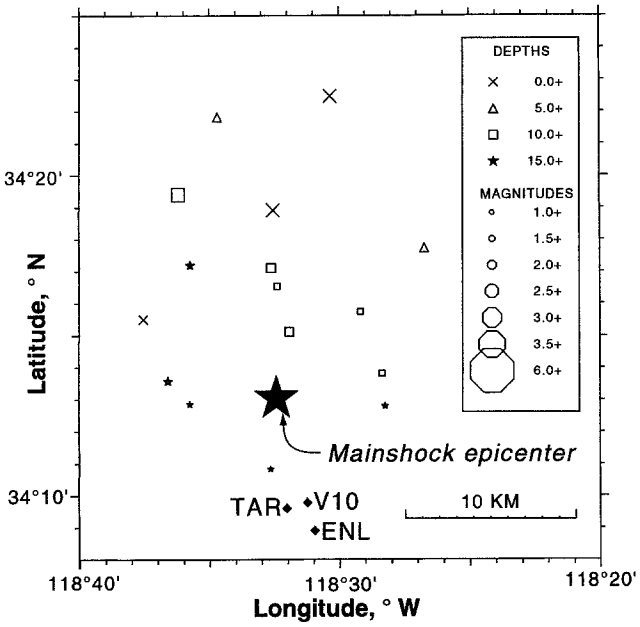

Figure 1. Map showing the epicenters of the Northridge mainshock (large star); the 16 aftershocks used in this study; and the locations of accelerographs at the Cedar Hill Nursery (TAR), the Encino Reservoir left abutment (ENL), and the Ventura Boulevard Building 10 (V10).

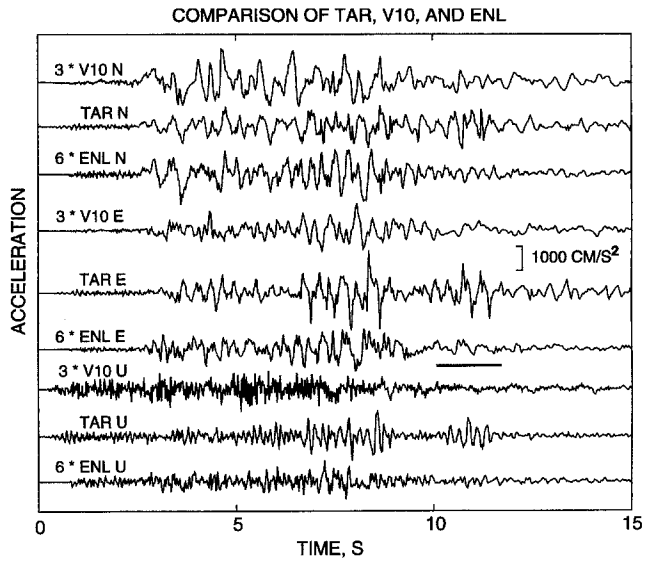

Figure 2. Ground accelerations recorded at TAR, ENL, and V10 during the Northridge earthquake. V10 and ENL motions have been multiplied by factors of 3 and 6, respectively. Note large accelerations on the east component of TAR. Horizontal bar from 10 to 12 sec indicates a third seismic arrival.

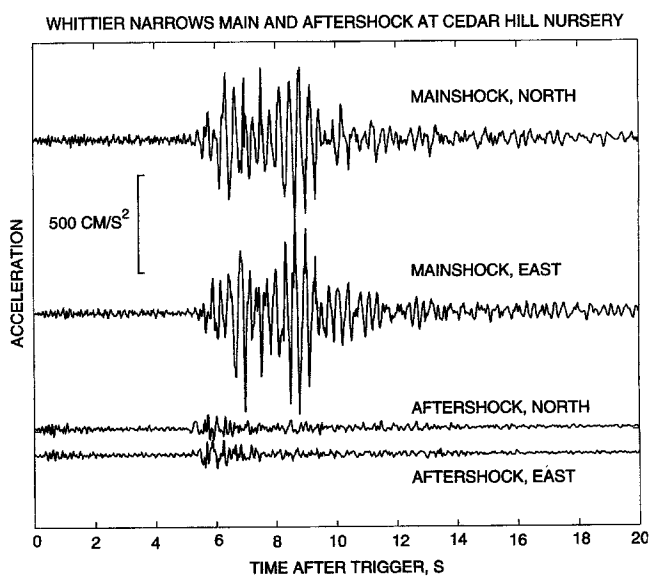

Figure 3. Horizontal ground accelerations recorded at the Cedar Hill Nursery (TAR) during the 1987 Whittier Narrows mainshock (87/10/1 14:42, M_L 5.9) and its largest aftershock (87/10/4 10:59, M_L 5.3).

10 higher than was observed at most other sites at an equal epicentral distance, and it was considerably higher than expected from empirical acceleration attenuation curves (Shakal *et al.,* 1988). Surprisingly, the Tarzana peak accelerations observed in the largest Whittier Narrows aftershock were only a factor of 2 larger than that observed at stations having similar epicentral distances (Fig. 3). The large discrepancy between the Tarzana ground motions in these two events has not yet been explained.

To help understand the Tarzana ground motions, Lee *et al.* (1994a, 1994b, 1994c) deployed a dense array of seismometers around the site and recorded weak motions from Northridge aftershocks. In this article, we analyze the weak-motion data as well as the strong-motion data, and we provide a more complete description of the site's amplification, its relationship to topography, its spatial extent, and its relationship to earthquake source effects.

Site Description

The California Division of Mines and Geology (CDMG) accelerograph at the Cedar Hill Nursery (station number 24436, henceforth referred to as TAR) is located at the east end atop a natural hill about 15-m high, 500-m long, and 130-m wide, striking about N78°E (Fig. 4). The hill is mapped as the upper part of the Modelo Formation by Hoots (1931) (Fig. 5) and Dibblee (1992) and is Miocene in age. Strike of the beds is approximately parallel to the hill strike, and the beds dip northward at about 30°. The Modelo Formation is covered in some places by a thin veneer of sediments and fill. Detailed geologic mapping by Geosoils (1992) shows the top of the hill, upon which the Tarzana SMA sits, to be covered by 1 to 2 m of artificial fill. The Modelo Formation is exposed on the flanks of the hill, while the base is covered by 1 to 2 m of Quaternary slope wash, i.e., materials eroded from the flanks of the hill. Hoots (1931) shows a possible fault running along the southeast side of

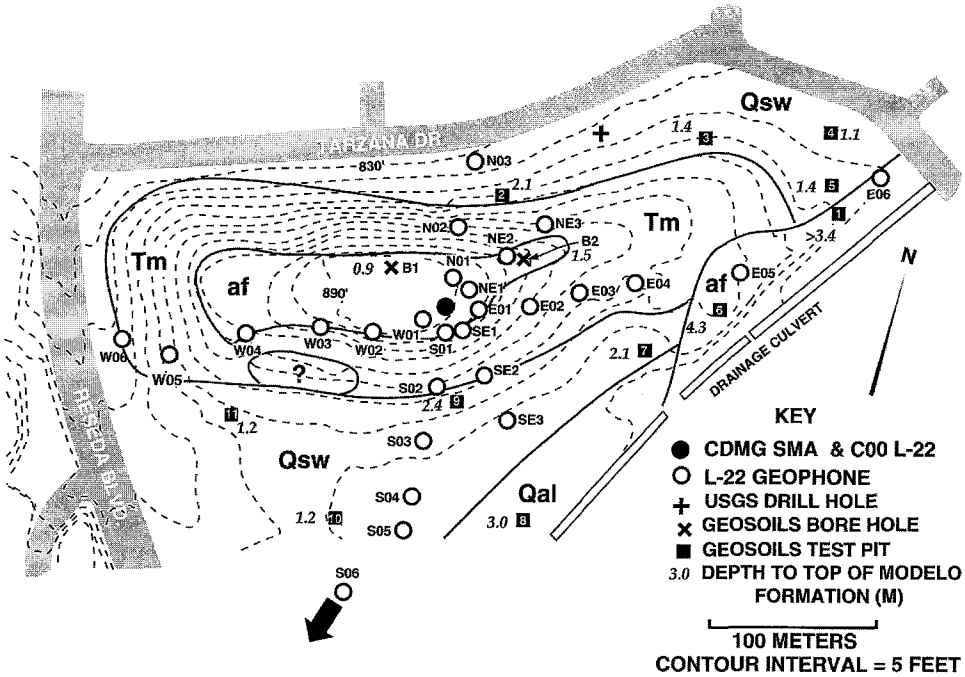

Figure 4. Map of topography (dashed contours), surface geology, and instrument layout, Cedar Hill Nursery, Tarzana. Open circles show geophone locations; solid circle shows geophone C00 and the CDMG accelerograph TAR. Cross shows corrected location of the Fumal *et al.* (1981) drill hole. Black numbered squares are pits dug by Geosoils (1992) for mapping purposes, and italic numbers are depths to Modelo Formation, in meters, observed in pits and boreholes. Locations of geologic contacts (solid lines) are approximate. Map-unit symbols: af, artificial fill; Qsw, slope wash (Quaternary); Qal, alluvium (Quaternary); Tm, Modelo Formation (Miocene). "?" denotes a geologic unit not identified by Geosoils (1992). S06 was about 300 m southeast of S04 in direction of arrow.

the hill, and Geosoils (1992) shows a drainage along the same side of the hill. Natural Quaternary alluvium having a depth of 3 m lies along part of the drainage, while artificial fill, possibly emplaced during construction of a drainage culvert, lies along the northeast portion of the culvert, where depth of the artificial fill may exceed 4 m. The facilities of the Cedar Hill Nursery lie between the culvert and Tarzana Drive on the eastern 150 m of the property.

Fumal *et al.* (1981) drilled and logged a site about 140 m from the Tarzana SMA (Fig. 4) [Note that the location of this hole given in Fumal *et al.* (1981) is incorrect. Figure 4 shows the correct location (T. Fumal, personal comm., 1994).] They identified the upper 6 m as consisting of a silty clay loam and deeply to moderately weathered shale, and the interval from 6 m to the bottom of their hole at 30 m consisted of soft to firm shale. *P*- and *S*-wave arrival times, measured by Fumal *et al.* (1981) using a surface seismic source and a downhole seismometer, show average *P* and *S* velocities of 744 and 369 m/sec, respectively, to a depth of 20 m.

Northridge Aftershock Data

On 10, 11, and 12 February 1994 (days 41, 42, and 43), an array of seismometers was deployed on the hill to record aftershocks of the Northridge earthquake (Lee *et al.*, 1994a, 1994b, 1994c). A 3-component Mark Products L-22 2-Hz-velocity geophone was deployed at each site on Figure 4, and all geophone channels were connected by wire to a centrally located 64-channel 16-bit digitizer and recorder. Each channel was sampled at 100 samples/sec. All sensors were oriented to geographic north. More details of the instrumentation and experimental design can be found in Lee *et al.* (1994a, 1994b, 1994c).

The basic layout consisted of six radial lines of instruments, nominally to the north (N), south (S), east (E), west (W), northeast (NE), and southeast (SE). In addition, an L-22 was emplaced at site C00, located about 2 m from the Tarzana SMA. Not all sensor sites were occupied simultaneously: on 10 February, only the N and S lines were occupied (C00 was not occupied); on 11 February, the N, S, E, and W lines as well as C00 were occupied; and on 12 February, the N, NE, E, SE, and S lines and C00 were occupied. Amplifier gains were a factor of 10 lower on 12 February than on the preceding days, so larger events were recorded without clipping on that day. Instrument locations were surveyed using a total station theodolite.

We selected 16 aftershocks for analysis. Our criteria for selection were that C00 (cosited with the Tarzana SMA) pro-

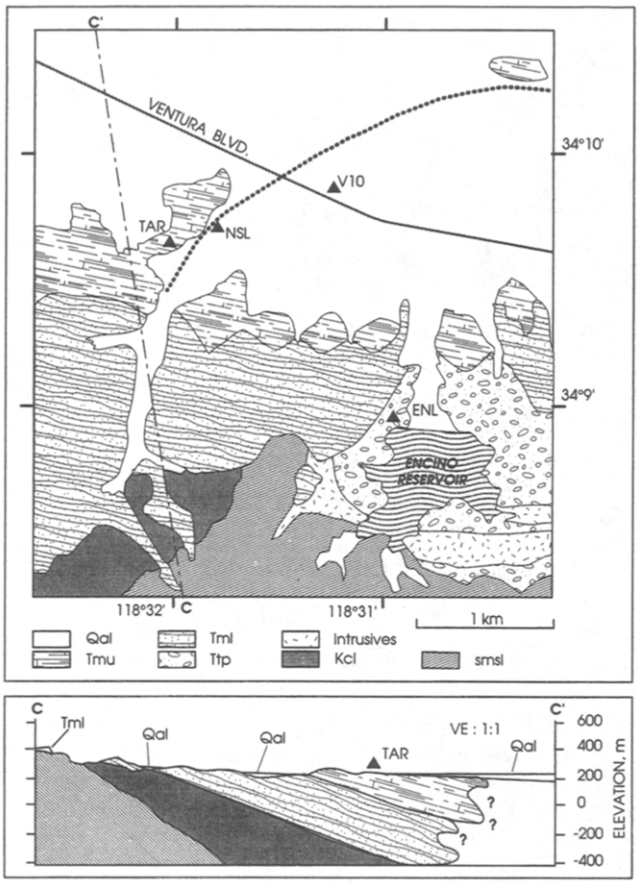

Figure 5. Geologic map and cross section, taken from Hoots (1931) with modifications from Dibblee (1992). Accelerographs TAR, V10, and ENL are shown. A portable seismograph was deployed at NSL by Wennerberg *et al.* (1994). Dotted line shows inferred fault mapped at east end of hill. Map unit symbols: Qal, alluvium (Quaternary); Tmu, Tml, upper and lower Modelo Formation (Miocene), respectively; Ttp, Topanga Formation conglomerate (Miocene); Kcl, conglomerate (Cretaceous); smsl, Santa Monica slate (Jurassic?).

duced a usable record and that the data were as large as possible without clipping. In a few cases, some seismograms were slightly clipped, but the clipping was so minimal that we do not believe the results of the analysis were affected. Epicenters of the 16 events are shown in Figure 1, and hypocentral coordinates and mechanisms are given in Table 1 (Egill Hauksson, personal comm., 1994; Hauksson *et al.*, 1995). An example of the time series from one aftershock is given in Figure 6. For convenience, henceforth we will refer to events by their day of the year and origin time (e.g., 11 February 0529 UTC is 0420529). It should be noted that peak velocities of most events recorded on day 042 and 043 were about 0.01 and 0.1 cm/sec, respectively. These are factors of 10^{-4} and 10^{-3}, respectively, of the peak velocities during the mainshock at TAR. Consequently, ours is definitely a weak-motion study.

Polarization Analysis

Method

Many important site-response and source characteristics can be understood through polarization analyses of the aftershock and mainshock motions, either as simple particle motion plots or as frequency-dependent polarization analyses. For the latter, we used the expressions in Vidale (1986), with a modification. Vidale's analysis is posed in the time domain, using a covariance matrix that is a function of time (his equation 3). Our modification was to use instead a covariance matrix that was a function of frequency, obtained analogously to Vidale's equation (3) from products of the appropriate complex Fourier spectra of the time signals. To help stabilize results, we smoothed the covariance elements as a function of frequency by convolving each element by a boxcar function having a bandwidth of 0.5 Hz. All of Vidale's subsequent equations for polarization strike, dip, ellipticity, etc., were used without modification.

Polarization Analysis of Strong Motions

Simple particle motion plots (Fig. 7) of the strong motions at TAR recorded in several earthquakes suggest that the site has a dominant direction of motion of about N140°E. Motions at TAR during the $M_L = 5.9$ Whittier Narrows mainshock and its largest aftershock, $M_L = 5.3$ on 4 October 1987, show the dominant direction of motion in both of these events to be about N140°E (Vidale *et al.*, 1991), although it is not clear from these records that this observed directionality is a property of the Tarzana site, rather than a source effect, because the expected polarization of both events is in approximately this direction (Vidale *et al.*, 1991). The same dominant direction of motion is seen in particle motions of the Sierra Madre earthquake recorded at TAR (not shown). This dominant direction also appears in most time windows of the Northridge mainshock records recorded at TAR (Fig. 7), except for the time windows containing the largest peaks, between 6.5 and 12.5 sec after trigger, which are more east–west polarized. The fact that the N140°E motions appear in most time windows of four earthquakes recorded at TAR, particularly in coda windows, suggests that this dominant polarization is a property of the site. By contrast, Northridge mainshock particle motions at Encino Reservoir left abutment (ENL, Fig. 5) are dominantly north–south oriented during the entire event. Mainshock particle motions at Ventura Boulevard building #10 (V10, Fig. 5), located about 1 km from TAR, are also predominantly north–south, except during the 6.5- to 8.5-sec time window (the window during which TAR experiences its largest east–west motions), when substantial east–west energy is present (Fig. 7). Figure 8 shows that the Northridge mainshock horizontal accelerations have most of their power between about 1.5 and 4 Hz and that in this frequency band, the motions are strongly polarized in the N120°E direction, which is consistent with the easterly particle motions seen in the 6.5- to 12.5-sec in-

Table 1
Event Hypocenters, Mechanisms, and *S* Polarizations

Date	Day	Origin Time (UTC)	Latitude	Longitude	Depth (km)	*M*	Dip Dir*	Dip†	Rake‡	*h*§
Feb 10	041	0446:40.66	34° 13.57′	−118° 36.61′	19.78	2.3				
Feb 10	041	0645:25.70	34° 22.47′	−118° 30.34′	4.50	2.5				
Feb 10	041	0712:50.43	34° 15.74′	−118° 29.18′	13.31	1.8				
Feb 10	041	1258:42.94	34° 17.11′	−118° 32.63′	11.43	2.0				
Feb 11	042	0529:03.29	34° 15.12′	−118° 31.93′	14.01	2.0	150	60	−30	85
Feb 11	042	0557:50.10	34° 17.73′	−118° 26.72′	9.20	2.1	215	30	110	−10
Feb 11	042	0610:22.74	34° 17.19′	−118° 35.75′	16.29	2.4	210	60	170	−27
Feb 11	042	0747:29.66	34° 12.85′	−118° 35.77′	19.75	1.7	150	30	130	−72
Feb 11	042	0836:59.24	34° 21.82′	−118° 34.69′	6.01	2.1				
Feb 11	042	1219:21.52	34° 15.50′	−118° 37.54′	1.42	2.0	125	70	30	71
Feb 11	042	1329:45.02	34° 16.53′	−118° 32.39′	10.22	1.7	170	20	50	71
Feb 11	042	1435:44.93	34° 13.81′	−118° 28.35′	13.16	1.9				
Feb 12	043	0152:52.41	34° 12.80′	−118° 28.24′	17.71	1.7				
Feb 12	043	0658:48.69	34° 19.39′	−118° 36.21′	12.24	2.5	185	55	70	13
Feb 12	043	1052:24.11	34° 10.83′	−118° 32.66′	16.73	1.9	220	45	120	−24
Feb 12	043	1510:30.44	34° 18.91′	−118° 32.55′	2.78	2.9	255	85	170	98

*Downdip azimuth, degrees clockwise from north.
†Dip angle, degrees from horizontal.
‡Rake, degrees: 0 = left-lateral; 90 = reverse.
§Direction of *S* motion in horizontal plane, degrees clockwise from north.

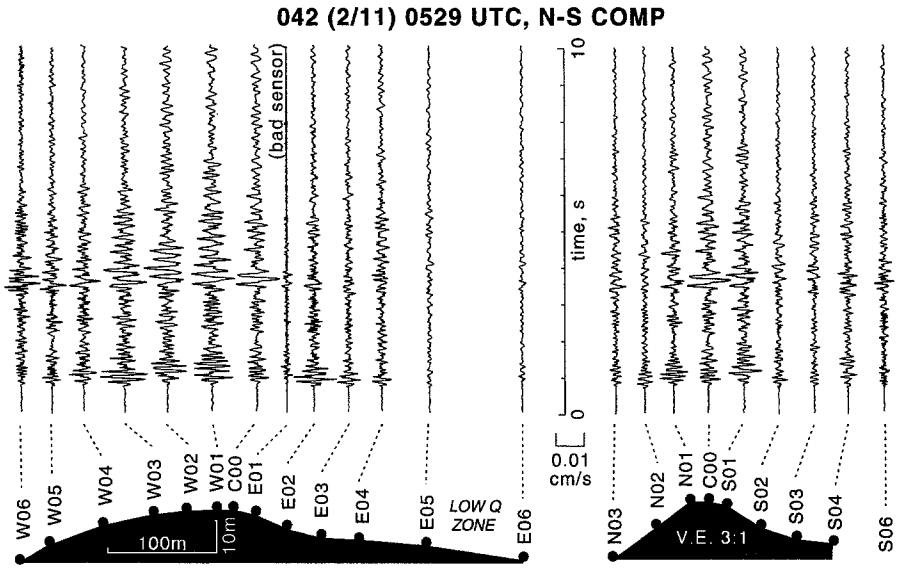

Figure 6. North–south component seismograms from the *M* 2.0 0420529 aftershock recorded on the east–west and north–south instrument lines, with instrument elevation profiles shown at bottom. C00 record displayed twice. Note low amplitudes at E05 and E06 caused by a zone of low Q, and note, especially, variation in *S*-wave amplitude along the N03-S06 line. S06 was about 300 m southeast of S04.

terval in Figure 7. It is important to note that this direction is not transverse to the long axis of the hill (Fig. 4).

Polarization Analysis of Aftershocks and Comparison with Mainshock

Confirmation of a directional site resonance at the Tarzana site comes from frequency domain polarization analyses of 12 aftershocks recorded at C00 on days 042 and 043. An example of this analysis is shown for the 0420529 aftershock in Figure 9. For these analyses, time windows of 5-sec duration were typically used, starting about 1 sec before the *S* wave. This length was adequate to include the *S* wave and the large amplitude *S* early coda, which is presumably a site response. A cosine taper was applied to the first and last 0.5 sec of the window. These aftershock polarization analyses show a very similar pattern of polarization direction

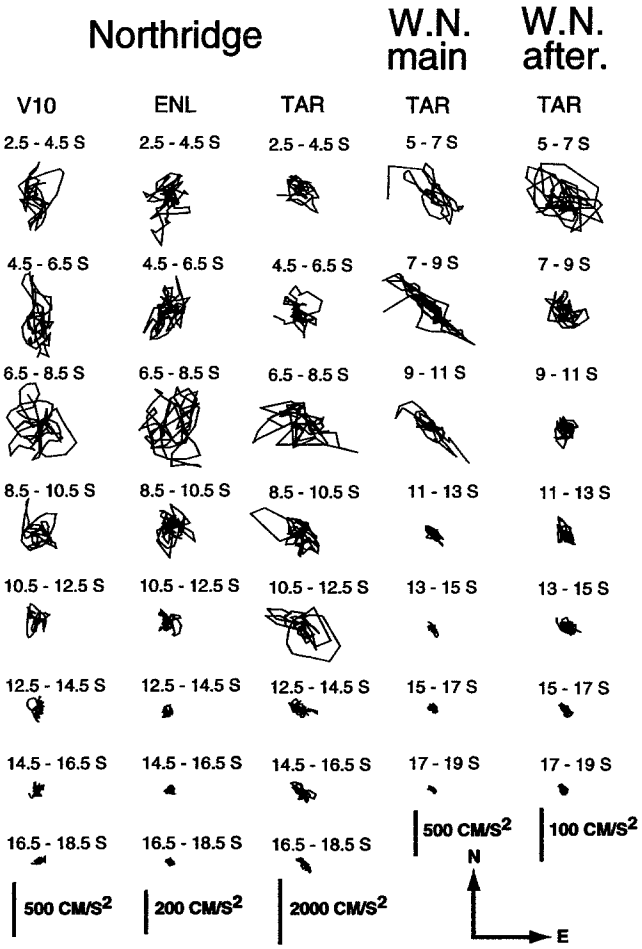

Figure 7. Particle motion plots for accelerograms recorded at V10, ENL, and TAR during the Northridge mainshock and at TAR during the 1987 Whittier Narrows mainshock and its largest aftershock. Each plot is for a successive 2-sec duration window. Time annotated above each panel is time after trigger. Amplitude scales are at the bottom of each column. Whittier Narrows events show a strong polarization at TAR along N140°E. Early (2.5 to 4.5 sec) and late (14.5 to 18.5 sec) windows of Northridge at TAR also show the same polarization, which is a site characteristic, but intermediate windows (6.5 to 12.5 sec) show a more easterly polarization. Early windows (2.5 to 6.5 sec) of the Northridge shock at V10 and ENL show dominant north polarization. Substantial, but not dominant, east-polarized energy arrives during the 6.5- to 8.5-sec window at V10 and ENL.

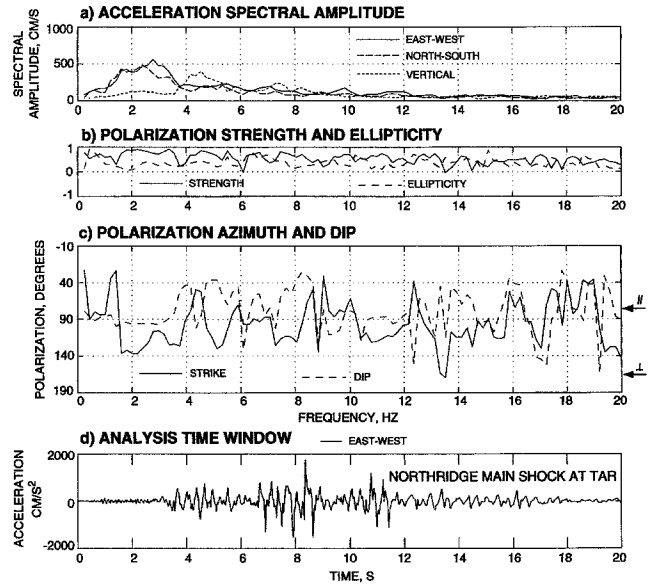

Figure 8. Polarization analysis for Northridge mainshock at TAR. (a) Amplitude spectra of three components of motion. (b) Polarization strength and ellipticity. (c) Strike and dip of the direction of maximum polarization. Parallel and perpendicular symbols on right indicate directions parallel and perpendicular to the long axis of the hill. (d) Portion of the 3-component time series used in the analysis (only east–west component shown). Note between 1.5 and 4 Hz, the ground motion is strongly polarized along the N120°E direction.

as a function of frequency from aftershock to aftershock, regardless of the expected *S* polarization (Fig. 10), as has been observed previously by Bonamassa and Vidale (1991), Bonamassa *et al.* (1991), and Vidale *et al.* (1991). Expected polarization was determined by using aftershock focal mechanisms (E. Hauksson, personal comm., 1994) and by ray-tracing *S* waves in the velocity structure of Wald and Heaton (1994). Interestingly, the Northridge mainshock polarization agrees fairly well with the aftershock polarizations at most frequencies, although in the 1.5- to 4-Hz band, where the mainshock spectral peak is located, the mainshock polarization is more easterly than the aftershocks.

Particle motion plots for all stations from several aftershocks show that the directional characteristics of the ground motions are strongly influenced by the topography of the site. As will be justified in greater detail in a later section, it appears that the hill has a strong mode of oscillation in which the top of the hill moves transverse to the long axis of the hill. However, this oscillatory mode does not explain the particle motions completely. Figure 11 shows particle motions in map view for four aftershocks. The particle motions have been calculated from time series that have been low-pass filtered at 4 Hz using a zero-phase Butterworth filter.

A common feature of all these particle motion plots is that polarizations of stations at the top of the hill (C00, W01, W02, W03) are always oriented more nearly transverse to the strike of the hill than are motions at the base and flanks of the hill, regardless of the theoretical polarization. This observation is consistent with the idea that the transverse mode of oscillation is strongest at the hilltop stations. In Figure 11a, the theoretical polarization is nearly east–west, and polarizations of stations at the ends of the radial station lines lie at azimuths between N100°E and N130°E. However, the azimuth of C00, W01, W02, and W03 is N140°E or more. (We suspect that the azimuth of W02 may be biased by a weak east–west data channel because observed particle

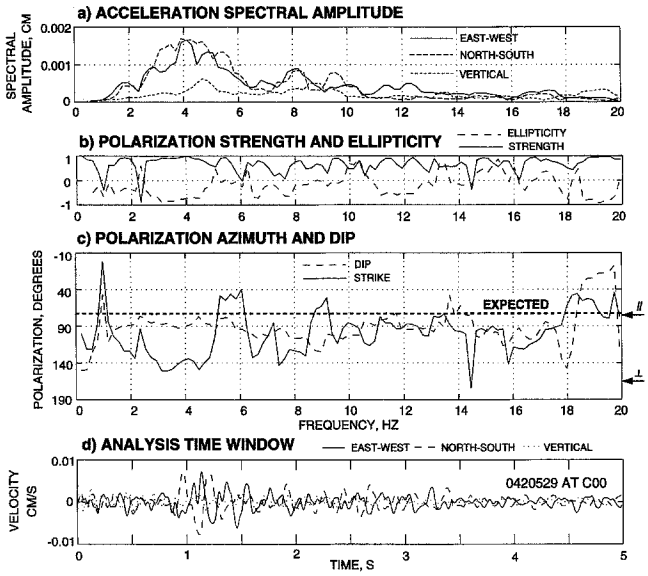

Figure 9. Polarization analysis for aftershock 0420529 at C00. (a) Amplitude spectra of three components of motion. (b) Polarization strength and ellipticity. (c) Strike and dip of the direction of maximum polarization. Parallel and perpendicular symbols on right indicate directions parallel and perpendicular to the long axis of the hill. (d) Portion of the 3-component time series used in the analysis. Arrow on right shows expected polarization strike. Note between 2 and 4 Hz, the ground motion is strongly polarized along the N140°E direction.

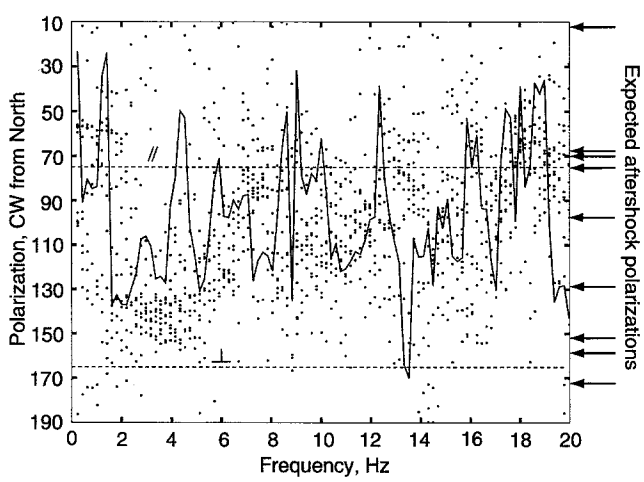

Figure 10. Polarization strike as a function of frequency, for 12 aftershocks at C00 (dots) and for the Northridge mainshock (line, from Fig. 8). Arrows on right are theoretical aftershock polarizations where known. Aftershock polarizations agree with each other fairly well and do not agree with expected polarizations. Mainshock polarization generally agrees with aftershock polarizations, although it is more easterly in the 1.5- to 4-Hz band where most mainshock power lies. Parallel and perpendicular symbols indicate directions parallel and perpendicular to long axis of hill.

motions for all investigated events vary smoothly from C00 to W06, except for W02, which always has more northerly particle motions.) Figure 11b shows the hilltop stations' polarizations to be more nearly perpendicular to the hill than the polarizations at stations at the extreme ends of the instrument lines. Figure 11c shows the only one of the 12 aftershocks studied in which the polarization of C00 is not approximately N140°E. However, even in this case, the C00 polarization is more transverse to the strike of the hill than are the polarizations of the other stations. Figure 11d shows a similar behavior to Figure 11a.

Although these hilltop stations have polarizations that are more nearly transverse to the hill than do the lower stations, it should be noted that their particle motions are not exactly transverse to the hill. Averaged over all 12 aftershocks, the C00 particle motion orientation is about N140°E, and averaged over eight aftershocks, the W01 and W03 orientations are about N150°E and N135°E, respectively. The azimuth transverse to the hill is about N168°E, so these hilltop stations have particle motion orbits rotated about 20° to 30° away from the transverse.

We checked the particle motions for evidence of material anisotropy, but we found none. No clear shear-wave splitting was observed, and although elliptical particle motions were occasionally observed, they were not consistent with a single anisotropic axis from event to event.

Comparison of Aftershock Base and Hilltop Motions

The foregoing particle motion analyses do not completely isolate the directional properties of the topographic effect because all the motions, both base and hilltop, are biased by the characteristics of the unknown incident *S* wave and perhaps by a more regional directional effect common to all stations. A clearer picture of the effect of topography, both on the amplitudes and the polarizations of ground motions, can be obtained by looking at ratios of hilltop-to-base motions. Before summarizing the aftershock results, it is important to note that top/base spectral ratios are not measurements of absolute amplifications with respect to a half-space. Motions at stations at the base of a hill can be amplified or more commonly deamplified by outgoing waves diffracted from the top of the hill (Bard, 1982), and it is possible that none of our base stations was sufficiently far from the hill to be completely unaffected by the presence of the hill. It should also be noted that if a common directional signal is present at both the base and the top of the hill, it will disappear when top/base spectra ratios are taken.

Spectral Ratio Method

We determine aftershock source spectra and station site-response transfer functions by applying a modified version of the inversion method of Andrews (1986) and Boatwright *et al.* (1991) to the ensemble of seismograms at all stations for the 16 aftershocks. Briefly, in this method, the log of the observed Fourier power spectrum of each record is ex-

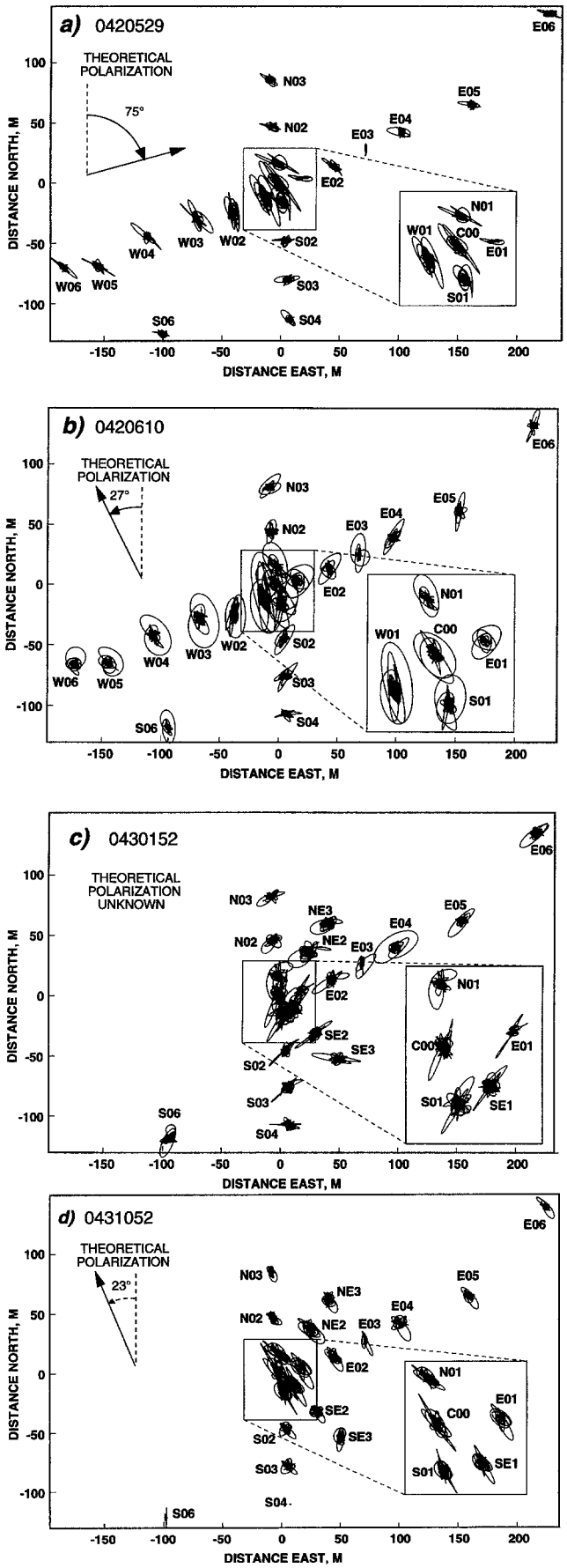

Figure 11. Maps of particle motions for four aftershocks. All time series filtered with a low-pass filter at 4 Hz. Insets show C00 and nearby stations. Arrow shows expected polarization, when known. W02 east channel may be weak in all plots. (a) Aftershock 0420529, E03 east channel dead. (b) Aftershock 0420610. (c) Aftershock 0430152. This is the only event of the 16 studied having substantially different polarization at C00. S04 north channel may be weak. (d) Aftershock 0431052. S04 dead, S06 east channel dead.

pressed as a sum of the log of an unknown earthquake source spectrum and the log of an unknown site-response spectrum. Because an arbitrary function of frequency can be added to the source spectra and subtracted from the site-response spectra in such a way that the data are not altered, we assume that site C00 has a flat site-response spectrum. The relationship between the spectra can be expressed as a linear matrix problem, and it can be solved for the source spectrum of each aftershock and for the ratio of each station's site-response spectrum to that of C00. For brevity, we will refer to this Source Spectra and Site Effects Inversion method as the "SSSEI." In Andrews (1986) and Boatwright *et al.* (1991), the SSSEI was performed on spectra that were averaged over finite-width frequency bands, with the ratio of upper-to-lower frequency in each band being $2^{1/4}$, i.e., 4 bands per octave.

We have made three changes to the inversion method. First, we used a slightly different definition of the errors in the ground-motion spectra, because equations (3) in Boatwright *et al.* (1991) and (4) in Andrews (1986) do not include the effects caused by use of spectra averaged over variable-width frequency bands. There has been some controversy (e.g., Field and Jacob, 1995) over error estimates in SSSEI methods. For brevity, we simply present without derivation the error estimate we used. This estimate has been verified by numerical testing with artificial signals having known noise components. Specifically, if V is the sum of ground velocity power spectra from c components of motion ($c = 1$ or 2), integrated over a particular frequency band, then s, the standard deviation of the $\log_{10}$ of V, is

$$s = \frac{2^{(2-c)/2}\,\eta}{2.3\sqrt{L}}, \tag{1}$$

where η is the ratio of the noise amplitude spectrum to the signal amplitude spectrum, $L = \max(n_I, 1)$, and n_I is the number of independent frequencies in the frequency band. Typically, a good estimate of n_I is n_T, the number of time samples in the signal time window, before padding with zeros, used to obtain V. To some extent, our use of s as defined in equation (1) is cosmetic, because we evaluate σ_k in equation (3) of Boatwright *et al.* (1991) using $\sigma_k = \max(s, 0.5)$,

meaning that σ_k is 0.5 for all but the worst data. Consequently, we have verified that our estimated uncertainties in the source spectra and site-response spectra obtained from the SSSEI are conservative, as are those of Andrews (1986) and Boatwright *et al.* (1991). Unfortunately, it is not possible to obtain less-conservative solution error estimates simply by reducing the 0.5 value in the definition of σ_k.

The second change to the inversion method was to choose a narrower bandwidth for each frequency band than was used by Andrews (1986) and Boatwright *et al.* (1991) in order to make our results more relevant to structural (building) response. Since the purpose of microzonation is ultimately to map predicted building response, it makes sense to study site response in frequency bands whose widths are comparable to the bandwidths of building resonances. Building response is often studied using a 5% damped harmonic oscillator model. If a 5% damped oscillator has its peak response at frequency f_0, then its response is down to 0.75 of the peak response at a frequency of about $1.05f_0$, or about $2^{1/14} f_0$. Consequently, in our work, the ratio of upper-to-lower frequency in each band was $2^{1/14}$ rather than the $2^{1/4}$ usually used.

The third change to the inversion method was to apply the SSSEI to ground-motion data directed only along a single horizontal component of motion, because we were interested in looking at the directional aspects of the response of C00. Usually, the SSSEI is applied to ground-motion spectra that are a sum of the spectra of the two recorded orthogonal components, obscuring any directional properties of the ground motion.

For actual application of the SSSEI, we chose a set of desired directions of ground motion spaced at 5° intervals in the horizontal plane. For each desired azimuth, the following steps were taken. We rotated the aftershock seismograms into that component of motion. As a noise estimate, we chose a 1.5-sec duration segment of ground motions in the rotated *P* coda, and as a signal estimate, we chose a 4.0-sec segment starting about 1.0 sec before the rotated *S*-wave arrival. The beginning and ending 10% of all data windows were cosine tapered, each data window was padded with zeros to 8192 points, and FFT's were taken. The SSSEI procedure, with the modifications to the error estimates described above, was then applied to the rotated noise and signal spectra for each desired azimuth.

Identification of Directional Resonances

In order to examine the response of C00 at the top of the hill compared with stations at the base, for each frequency band, we calculated the ratio R given by

$$R = \left[\frac{1}{B}\sum_{i=1}^{B} r_i\right]^{-1}, \qquad (2)$$

where there are B stations at the base of the hill and r_i is the amplitude spectral ratio of ground velocity at station i to that at C00, determined from the SSSEI. R is simply the inverse of the average base/top ratio for all base stations. In calculating R, we have taken stations E06, N03, S04, S06, W06, and SE3 to be at the base of the hill. We use the r_i determined from the SSSEI because for these station pairs, they are essentially identical to the base/top ratios that would be formed by direct division of observed spectra. It must be remembered that theoretical studies (e.g., Bard, 1982) show that ground motions at the base of a hill are sometimes diminished by the presence of the hill, so it is not necessarily true that the ratio R and the Tarzana mainshock record could be used to infer ground motions on the flatlands well away from the hill.

A plot of the ratio R as a function of frequency and azimuth of motion (Fig. 12) clearly shows directional resonances of C00 with respect to stations at the base of the hill. There are resonances parallel and perpendicular to the long axis of the hill, which is N78°E. The most prominent perpendicular resonances are at frequencies of 3.20 and 4.53 Hz, and they appear on Figure 12 as horizontal white streaks at the left and right sides of the diagram. Resonances parallel to the strike of the hill appear as faint horizontal white streaks having maxima in the center of the diagram at frequencies indicated by the open and filled dots.

It can be verified that the dominant resonances in Figure 12 are approximately parallel and perpendicular to the strike of the hill by plotting slices of the top/base ratio R at constant frequency. Figure 13 shows R as a function of azimuth of motion for frequencies at which horizontal white streaks can be seen, 3.20, 4.53, 5.80, 7.07, 8.62, 10.5, 12.2, 14.9, and 17.2 Hz. Assuming that the directional resonances should be separated by 90° in azimuth, approximate estimates of the best-fitting resonance directions are N75°E and N165°E, which agree within measurement error with the directions parallel and perpendicular to the long axis of the hill, N78°E.

While numerous possible resonances can be seen in Figure 12, we believe that only the perpendicular resonances at 3.20 and 4.53 Hz and the parallel resonances at 7.07 and 17.2 Hz are well resolved by the SSSEI. This can be seen by plotting the top/base ratio R and its error estimates as functions of frequency for two fixed azimuths of motion, N75°E and N165°E, approximately parallel and perpendicular to the hill (Fig. 14). Only at those four frequencies do the parallel and perpendicular top/base ratios differ by more than 2 standard deviations (filled circles, Fig. 12).

The SSSEI results and the particle motion plots strongly suggest that aftershock motions at C00 were amplified by a topographic effect. It appears that the 3.20-Hz resonance corresponds to the fundamental transverse oscillatory mode of the hill. This interpretation is consistent with the particle motions in Figure 11, which are low-pass filtered at 4 Hz and which show that motions at the top of the hill are larger than base motions and are rotated into a more northerly azimuth, owing to the strength of this resonance at the top of the hill. However, it is curious that particle motions at the top of the hill tend to be aligned along a N140°E azimuth

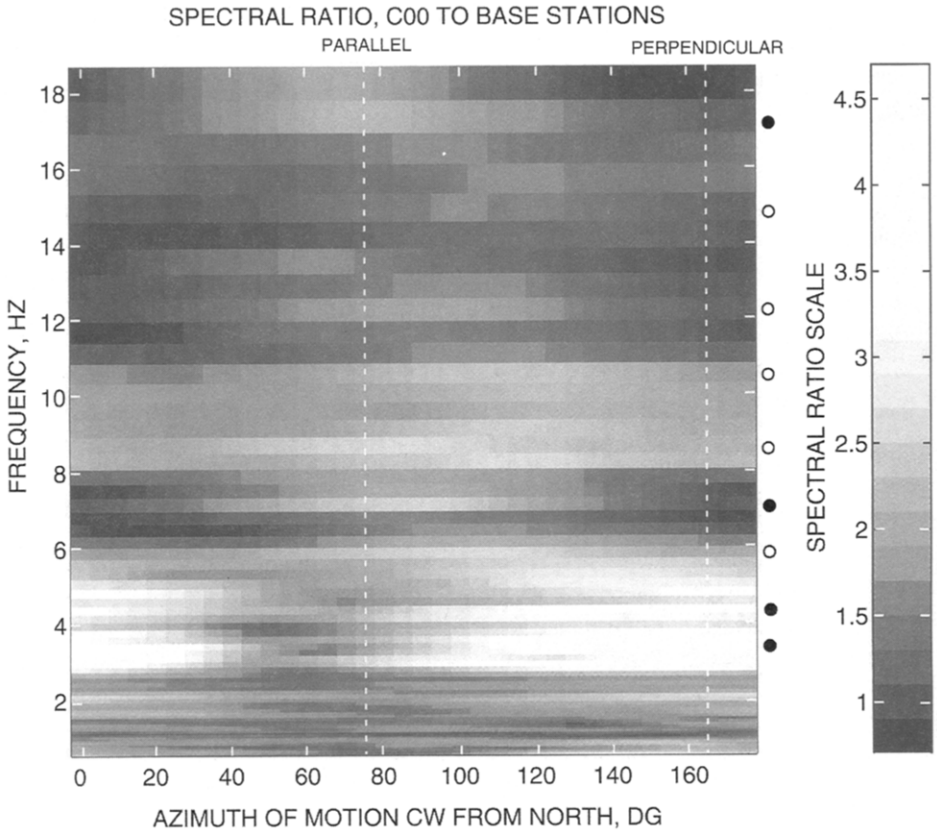

Figure 12. Average spectral ratio R (equation 2) of C00 to stations at base of hill (E06, N03, S04, S06, SE3, and W06), as a function of direction of ground motion. Vertical dashed white lines show directions parallel and perpendicular to long axis of hill. Filled circles on right indicate probable resonant frequencies; open circles indicate possible resonant frequencies. The horizontal white streak at 3.2 Hz is the fundamental perpendicular mode of the hill.

(Fig. 11) when the SSSEI-identified resonance is directed along N165°E. We will see below that there may have been an additional effect at work to cause this discrepancy.

Spatial Variation of Directional Site Responses

Figure 15 gives an overview of the main features of the directional site response function $r_i(f,\phi)$, the ratio of the ground velocity amplitude spectrum of the ith station to that of C00, as a function of center frequency f and direction of motion ϕ. For a fixed frequency and station number, this function can be plotted in a polar plot. The spatial variation of this function can be examined by plotting these polar plots on a map at their respective station locations, as in Figure 15. The interpretation of these plots is slightly counterintuitive because they depict ratios and not absolute amplitudes. For example, in Figure 15b, comparison of the C00 symbol and the N01 symbol (immediately north of C00) shows that at this frequency, the ground motion at N01 is nearly equal in amplitude to that of C00 for the N75°E component, but N01 is much smaller (or C00 is much larger) for the N10°E direction. In these plots, since C00 is the reference station, $r_i(f,\phi)$ for C00 is always a circle of unit radius. Ideally, a station having no prominent site response should be chosen as the reference station, but none of the stations deployed, including S06, satisfied this criterion.

The eight plots in Figure 15 are representative of the general features of the directional response of the stations. For frequencies below 2.5 Hz (Fig. 15a), stations higher on the hill have slightly larger (factor of 2) response than those at lower elevation, and directional properties are not strong, nor is there strong spatial variation of response. However, at 3.2 Hz (Fig. 15b), which we have associated with a transverse resonance of the hill, this resonance is strongest within a surprisingly short radius, 50 m, of C00 at the east end of the top of the hill. (Note in Fig. 15b, however, that motions in the N165°E direction at W02, W03, and W04 are still factors of 2 to 3 larger than at N03 or S04, so the 3.2-Hz resonance is not limited to the east end of the hill.) We do not understand why this resonance is most strongly concentrated at one end of the hill, and we cannot rule out lateral variations of geology as a contributing factor. At 4.5 Hz (Fig. 15c), the transverse resonance is less strongly concentrated at C00; it is seen at stations C00, W02, and W03. By 5.8 Hz (Fig. 15d), few directional resonances are seen. At frequen-

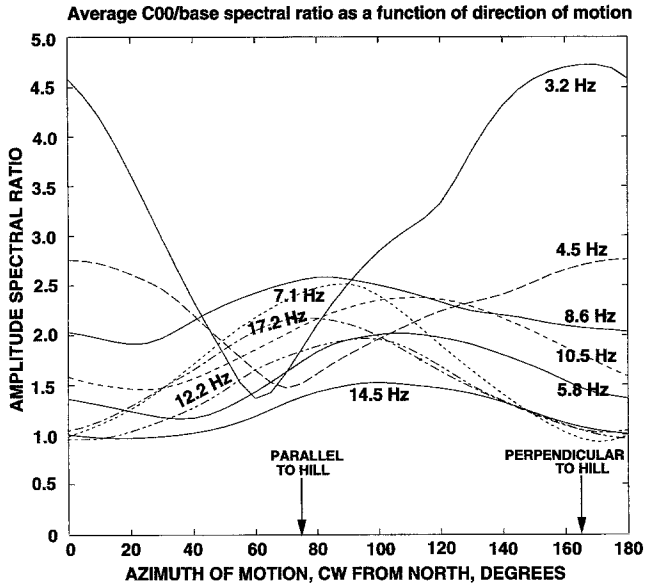

Figure 13. Horizontal slices through the function plotted in Figure 12, chosen at possible resonance frequencies (circles in Fig. 11). Directions parallel and perpendicular to the long axis of the hill are indicated. Resonances at 3.2 and 4.5 Hz are perpendicular to hill, others are parallel.

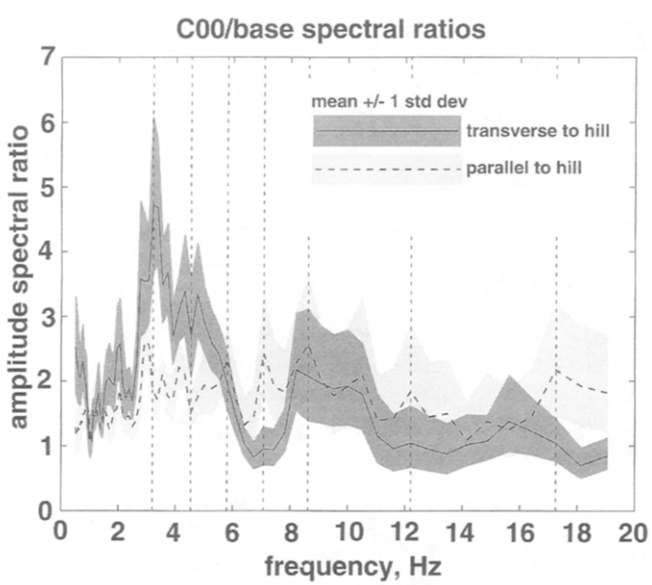

Figure 14. C00/base spectral ratios as a function of frequency, for azimuths of N75°E (solid line) and N165°E (dashed line). Gray bands are 1 standard deviation error bounds. Vertical lines correspond to frequencies shown in Figure 13. Note that only for frequencies of 3.2, 4.5, 7.1, and 17.2 Hz do the error bounds for the two azimuths fail to overlap (these frequencies shown as filled circles in Fig. 12).

cies of 7.1 Hz (Fig. 15e) and above, three important phenomena are visible. First, the responses of E05 and E06 are strongly attenuated; compare, for example, E05 and E06 to W05 and W06 at these frequencies and at lower frequencies. Second, spatial variation of response becomes larger. Third, for the N and S station lines, the response at the top of the hill and at the base (N03, S03, S04) tends to be larger than the response at the intervening stations on the hill slope. We do not understand the detailed pattern of responses in Figures 15e through 15h.

Estimating Lateral Variations of Geology

As seen above, there are substantial lateral variations of seismic response around the site that could conceivably be caused either by topography or by lateral variations of surficial or subsurface geology. Geosoils (1992) has provided measurements of depth to bedrock (Modelo Formation) at several places on the hill, but we have no estimates of depth to bedrock at most of the seismic stations including C00, nor do we have direct evidence of lateral variations of material properties within the bedrock.

To look for lateral variations of subsurface geology, we determined *S*-wave station delays. We used cross-correlation to measure relative arrival time delays on the east–west components of all stations for six aftershocks having impulsive *S*-wave arrivals, 0420610, 0420747, 0420836, 0421329, 0431052, and 0431510. It was necessary to use only the E–W component because the N–S component waveforms varied excessively from station to station because of differing contributions of the transverse resonance of the hill. Cross-correlation was performed on time series that had been Fourier interpolated to eight times higher sampling rate, enabling millisecond measurement of time shifts. To convert these observations to site delays, we used the following procedure. Suppose we have N stations, and the ith station is located at $\mathbf{r}_i$, where the centroid of the stations is the origin of coordinates. Then, assuming a plane-wave incident on the near-surface zone from the jth source, the theoretical *S*-wave arrival time at the ith station in a uniform medium is $t_{ij} = \mathbf{s}_j \cdot \mathbf{r}_i + T_j$, where $\mathbf{s}_j$ is the slowness vector of the plane wave and T_j is the arrival time at the centroid of the array. The slowness vector has a magnitude equal to the reciprocal *S*-wave medium velocity, $1/\beta$, and it has an incidence angle γ_j away from the vertical and an azimuth of propagation θ_j in the horizontal plane, all of which are unknown. If $\tau_{ij} = o_{ij} - T_j$ is the observed difference of *S*-wave arrival time o_{ij} and

$$T_j = \frac{1}{N}\sum_{i=1}^{N} o_{ij},$$

then we seek to find the set of γ_j, θ_j, and β that minimize

$$e = \sum_{i,j} (o_{ij} - t_{ij})^2 = \sum_{i,j} (\tau_{ij} - \mathbf{s}_j \cdot \mathbf{r}_i)^2.$$

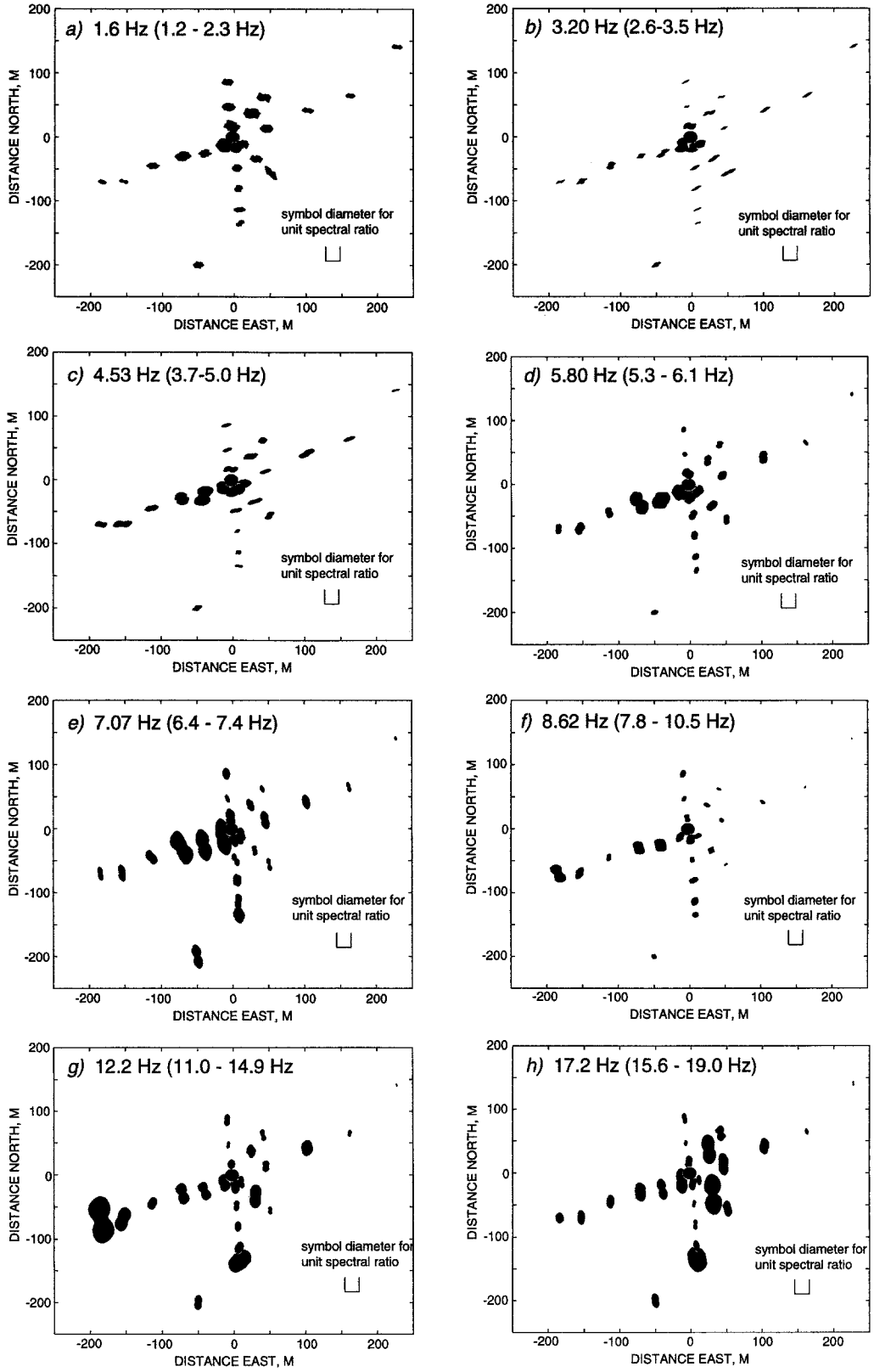

Figure 15. Spectral ratio of C00 to each station, as a function of frequency and direction of motion. Polar plot of spectral ratio is plotted at each station location. Radius is proportional to spectral ratio. See text for further details: (a) 1.6 Hz; (b) 3.2 Hz (note concentration of amplitude near C00); (c) 4.53 Hz; (d) 5.8 Hz; (e) 7.07 Hz; (f) 8.62 Hz (note small amplitudes at E05 and E06 compared to W05 and W06); (g) 12.2 Hz; (h) 17.2 Hz.

Since t_{ij} is nonlinear in β, we solve the nonlinear optimization problem using a modified grid-search algorithm, yielding the station delays for each source, which are the values of $d_{ij} = \tau_{ij} - \mathbf{s}_j \cdot \mathbf{r}_i$ at minimum e. Note that since $\mathbf{r}_i$ contains the station elevation, the resulting delays (Fig. 16) do not contain the effect of elevation differences. The uniform *S*-wave velocity that minimized the travel time error e was 0.47 km/sec, which is higher than the 0.37 km/sec average near-surface velocity we derived from the logging results of Fumal *et al.* (1981). However, the width of the minimum in the $e(\beta)$ curve is fairly broad, so we will continue to use Fumal's velocity. All *S* waves were observed to arrive within about 8° of vertical. We believe the station delays in Figure 16 are fairly reliable because the delays for each earthquake at a single station tend to agree, at least in sign; e.g., C00 is slow for all events, whereas N01 is fast.

The station delays are uncorrelated with known variations in sedimentary thickness, which can be roughly estimated from Figure 4 for 14 of the seismometer sites. An extreme example is given by E02, E04, and E05, for which sediment thicknesses are roughly 0, 0, and 4.3 m, respectively, and delays are about −0.012, 0.008, and −0.015 sec, respectively, with the deepest sedimentary site having early *S* waves. Assuming that the delay measurements are correct, this lack of correlation implies first that the sedimentary shear velocities are not so slow that they have a strong effect on delays and second that variations in the bedrock velocity, possibly caused by variable depth of weathering, may cause the *S* delays.

If the *S* delays are caused by shallow sediment or bedrock velocity variations, it might be expected that these variations might be accompanied by variations in impedance and ground-motion amplitudes. However, the delays in Figure 16 show no correlation with site-response amplitudes in any period band. We checked this correlation quantitatively by converting the *S*-wave delays to implied surface velocity variations in the top 30 m. These velocity variations implied variations in seismic impedance and consequent amplitude variations, which we calculated and compared to actual amplitude variations. No correlation was found in any individual frequency band or in results averaged over a band from 6 to 19 Hz, in which topographic resonances are small.

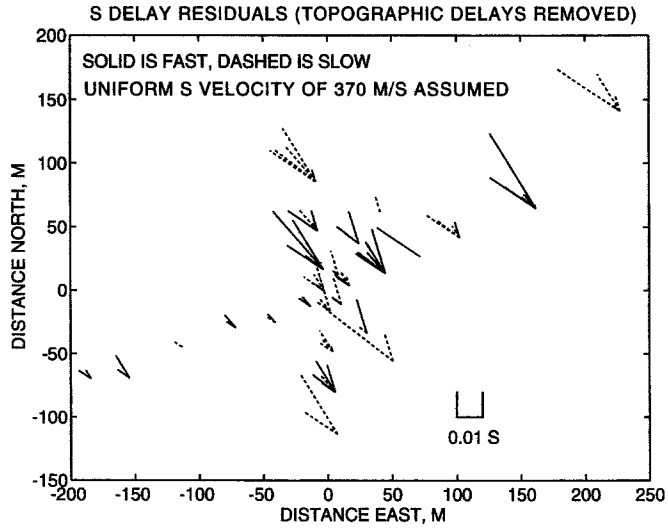

Figure 16. *S*-wave delays for six aftershocks, calculated using an assumed *S*-wave velocity of 0.37 km/sec. Each delay is plotted as a vector, with the south end of the vector at the station location. Each vector points back to the epicenter of the quake generating the *S* wave. Solid lines indicate negative delays (fast material velocities), and dashed lines indicate positive delays (slow material velocities). Delays caused by elevation differences have been removed. Delays do not correlate with elevation, surface geology, or ground-motion amplitude.

Discussion

The four most important aftershock observations relevant to the mainshock response of the hill are the directional resonances seen in the top/base spectral ratios (Fig. 12), the strong concentration of the 3.2-Hz resonance within 50 m of C00 (Fig. 15b), the low amplitudes observed at E05 and E06 above 6 Hz (Figs. 15e through 15h), and the tendency of aftershocks at C00 to be polarized along N140°E in the 2- to 4-Hz band (Fig. 10). We will discuss the causes of these in turn.

Several lines of evidence suggest that the 3.2-Hz resonance seen in the C00/base spectral ratios (Figs. 12 and 13) is topographic. First, its orientation is almost exactly perpendicular to the hill. Second, its frequency agrees with that expected from theory. Results from Bard (1982), Bouchon (1973), and Geli *et al.* (1988) indicate that the expected resonant frequency for transverse motion of a 2D ridge having a 0.37 km/sec *S* velocity and a width of 130 m is about 2.9 Hz, independent of shape ratio. Third, its peak amplification factor of about 4.5 is consistent with other observational studies summarized in Geli's Figure 2a, although the relief of our hill (shape ratio = 0.19) is considerably less majestic than that of most hills studied. Other resonances seen at higher frequencies (4.5, 7.0, and 17.2 Hz) are probably related to topography because of their orientations, but that is less certain. We have no explanation for the particular resonant frequencies.

Comparisons of our observations with theoretical results indicate that the 3D shape of the hill and its internal structure are important factors affecting its response. Surprisingly, studies of 2D hills, like Bouchon (1973) and Bard (1982), do not show the strong dominance of the transverse mode of oscillation over the parallel modes. Our observations indicate the importance of transverse oscillations of elongated 3D hills, and a theoretical study by Bouchon *et al.* (1995) confirms that the transverse mode becomes dominant in these hills. Bouchon and Barker (1995) have numerically simulated the response of a hill having the topography and seismic velocities of the Tarzana hill. Their numerical model shows the dominance of the transverse motions over the par-

allel, and their fundamental transverse resonance shows a top/base spectral ratio having a broad peak in the 3- to 4-Hz band, consistent with our 3.2-Hz observation. However, the fundamental transverse resonance peak in their model is much broader than our peak (Fig. 14) and has a maximum value of only about 1.6, compared to our peak of 4.5. This discrepancy strongly suggests that the internal structure of the hill is enhancing the transverse resonance. Consequently, in our observational study, and probably in many others, the observed "topographic" effect represents not only the effect of an irregular ground surface but also the correlated effect of the internal structure of the hill.

We have no good explanation for why the 3.2-Hz resonance is strongest within 50 m of C00. While most of the highest-amplitude sites are located on artificial fill (Fig. 4) of unknown thickness, the localized amplitude peak is probably not related to a vertical resonance in the soil layer under C00. If the fill had a shear velocity of 100 m/sec, it would have to be about 8.5-m thick to support a 3.2-Hz vertical resonance. This implies a 0.08-sec S delay, which we would certainly observe. In addition, the fill is less than 2-m thick where measured at boreholes B1 and B2. An alternate speculative explanation is based on the observation that stations W02, W03, and W04 are located at the south edge of the top of the hill, rather than very close to the crest like C00. Perhaps they are far enough from the crest that the upcoming S wave and the downgoing diffracted S interfere destructively at these sites, while not interfering at C00. This hypothesis is supported by the simulations of Bouchon and Barker (1995), in which ground-motion amplitudes at 3.2 Hz diminish rapidly over a very short distance, comparing sites on the top of the hill to sites on the flanks of the hill.

Two possible explanations for the attenuated ground motions at E05 and E06 above 6 Hz are low Q in the artificial fill underlying these sites, or presumed low Q in the fault zone they probably sit within (Fig. 5). While low Q in the artificial fill is undoubtedly a factor, we believe the presumed low fault zone Q is more important because the artificial fill seems to be too thin, at least where known at E05, to explain the observed diminution of high-frequency energy. For example, using conservative values of $Q = 5$ and S velocity $\beta = 100$ m/sec in the artificial fill, propagation of a 10-Hz S wave through 5 m of fill would reduce the wave amplitude to 74% of its initial amplitude. E05 and E06 amplitudes are considerably less than 74% of the E04, W05, and W06 amplitudes at frequencies above 6 Hz in Figure 15. It would be necessary to quadruple the fill thickness or to drop the Q to a value of 5/4 in order to explain the observed spectral ratios of E05 and E06 to E04, W05, and W06.

An important observation lacking a good explanation is the relative misalignment between the polarizations of the aftershock particle motions at the top of the hill (Fig. 11) and the polarizations of the top/base spectral ratios (Fig. 12). Aftershock ground motions (not top/base spectral ratios) at W03, W01, and C00 at the top of the hill tend to be oriented about N135°E, N150°E, and N140°E, respectively, i.e., 33°, 18°, and 28° away from the direction transverse to the hill, the predominant direction of the top/base spectral ratio at 3.2 Hz.

We speculate that the fault southeast of the hill striking N35°E (Fig. 5) may be causing this discrepancy by affecting the polarization of ground motions at the site. If the structural discontinuity at the fault caused scattered waves to be polarized transverse to the fault, and if these waves were present in approximately equal amounts at both the top and base of the hill, they would not be seen in the top/base spectral ratios, but they would cause all motions to be polarized in a more easterly direction. These scattered waves might alternatively be fault-zone-trapped waves (Cormier and Spudich, 1984; Li *et al.,* 1994). However, this explanation is very speculative because we have no evidence that the fault zone actually has low velocities, nor can we explain how such waves would be trapped from sources outside the presumed low-velocity channel.

Based upon our observations and the related theoretical work, we suggest that future investigators studying the effects of topography should place two or more seismometers far from the base of the hill studied, in order to avoid the zone of diminished motion at the base of the hill. In addition, seismometers should be placed at the center line of the hill rather than at a break in slope, in order to avoid the region of high spatial variation of ground motion (unless that is the effect being studied).

Implications for Understanding the Northridge Ground Motions at Tarzana

Given the previous discussion, it is highly surprising that the largest peaks in the Northridge mainshock record are polarized more east–west than any other polarization discussed in this article. Figure 7 shows that the entire Whittier Narrows record at TAR is polarized along ~N140°E, as are the earlier and later windows (2.5 to 4.5 sec, 14.5 to 18.5 sec) of the Northridge record. This was the dominant polarization of the aftershocks at C00. However, the mainshock window from 6.5 to 8.5 sec, having the largest motions, shows the most easterly polarizations.

We, like Çelebi (1995), believe that the Tarzana mainshock record is amplified by a topographic effect, but it is important to note that the 1.78 g peak acceleration is on the east–west component, and top/base spectral ratios for this component are only a factor of 2 or so (Fig. 14), so the topographic effect is modest for this component. Since base motions are sometimes deamplified by the hill, the factor of 2 may overestimate the amplification of motions at the top of the hill compared to nearby regions unaffected by the hill (assuming linearity of soil response).

We speculate that the predominance of east–west motions in the strongest part of mainshock at TAR (6.5 to 8.5 sec) was caused by substantial radiation of S waves having east–west polarization from the source, rather than by any peculiarity of the Tarzana site. While the ENL and V10 records were fairly strongly north–south polarized during the

2.5- to 6.5-sec interval (Fig. 7), they both show substantial, although not dominant, east–west motion during the 6.5- to 8.5-sec interval. Several strong-motion records south-southeast of the mainshock epicenter show larger east–west than north–south motions. Based on depictions of the available data in Wald *et al.* (1996) and Shakal *et al.* (1994), most of the stations to the south-southeast have data showing larger east–west motions (Stone Canyon Reservoir, the Wadsworth Veterans Administration Hospital, the Santa Monica City Hall, and the accelerations at Sepulveda Canyon Control Facility). The source of this east–west polarized energy is still not understood.

Mainshock accelerations on the east component at TAR are a factor of 2 larger than would be predicted from motions at ENL and V10, even if we consider the topographic effect at TAR and the probable variations of surficial *S*-wave velocity among these stations. Figure 2 shows that the rms TAR east accelerations are about 3.5 and 7 times larger than the V10 and ENL accelerations, respectively. V10 sits upon Quaternary alluvium, for which a 200 m/sec *S*-wave velocity is reasonable (Fumal *et al.,* 1981), and ENL sits on a well cemented conglomerate of the Topanga Formation, for which we estimate an *S*-wave velocity of 1050 m/sec, based on the velocity of hard conglomerate at Sky Terrace (Fumal *et al.,* 1981). Using these velocities, the empirical curves of Boore *et al.* (1994) for peak ground acceleration and for pseudospectral response in the 2-sec–10-Hz band predict that TAR should be about 0.75 and 1.6 times larger than V10 and ENL, respectively. Doubling these numbers to account for the topographic effect on the east component of TAR (assuming soil linearity) gives 1.5 and 3.2, values which are slightly less than half the observed amplitude ratios. A similar comparison for the north component is not so straightforward because the effect of the narrow-band transverse topographic resonance (Fig. 14) on the north component at TAR would have to be explicitly computed.

In addition to amplitude differences, the TAR, ENL, and V10 records differ in apparent duration. All records are similar in character up to about 9 sec after trigger, but subsequently, from 10 to 12 sec, a strong arrival is seen at TAR that is only weakly seen at ENL and V10. The presence of this arrival on all three stations indicates that it is probably a source effect, but we do not know why it is so much stronger at TAR.

The above amplitude comparison, as well as the polarization comparisons, show that there is some unidentified third factor, having a spatial scale larger than our aftershock array, that is affecting amplitudes and polarizations around TAR. This affected zone probably extends as far as station NSL (Nestle School, Fig. 5), a station deployed by Wennerberg *et al.* (1994), who report that C00/NSL spectral ratios are very similar to C00/E06 spectral ratios. However, this affected zone does not extend to V10.

We have seen that several different factors contribute to spatial and directional variations of ground motions over scales from 25 m to 2 km at the Tarzana site, complicating the problem of microzonation. First, variations in site geology, topography, and other unknown factors cause the factor of 7 difference in accelerations between the Encino Reservoir and Tarzana 2-km distance. Such differences make it difficult to draw a meaningful contour map of peak acceleration in the Los Angeles region without using site geology at a minimum to guide the placement of contours. Even then, such maps may have an irreducible factor of 50% standard deviation. Second, even minor hills having low shape ratios can cause substantial topographic effects if these hills are about 1 seismic wavelength in width. Even though our eyes are drawn to the tallest peaks in a hilly region, it may be that the largest topographic effects are associated with the smaller-scale wrinkles on the sides of the major peaks, depending on the surficial *S*-wave velocity. Topographic amplifications may be occurring on most of the hills in the Los Angeles region. These topographic amplifications may be damaging or harmless, depending on the relative resonance frequencies of the hills and the structures built upon them. Third, the presence of a strong directional resonance at a site does not prevent strong motions from occurring in other directions. Fourth, there can be lateral variations in motion along the tops of these hills on a scale of 50 m, possibly caused by the wave interference effects and the detailed shape of the hill. Fifth, we have seen that a strong lateral variation in attenuation, probably associated with a fault, caused substantially lower motion at frequencies above 6 Hz at sites E05 and E06. These frequencies are important for the response of 1- to 2-story structures, and our observation of high attenuation at the east end of the hill probably explains the curious observation that there was little mainshock damage at the plant nursery, located near E05 and E06 (Lee *et al.,* 1994b). Stacks of flower pots were not overturned at this location. Sixth, there may be some additional scattered waves associated with the fault zone and seen at both the base and the top of the hill. This scattered energy might account for part of the discrepancy between the TAR, ENL, and V10 mainshock motions. While the Tarzana site may represent an unusual coincidence of many of these geologic factors, each of them individually poses a challenge for microzonation.

Acknowledgments

We thank landowner Ralph Herman Sr. for his unhesitating permission and assistance in carrying out this work and A. F. Shakal for his cooperation in instrumenting his accelerograph site. We also thank David Wald for providing much unpublished information about his mainshock model; Craig Davis, Duane Buchholz, and James Wickser for supplying geologic information and the digital accelerogram from the Encino Reservoir site; Robert Darraugh for helping us acquire useful CDMG accelerograms; Robert Sydnor and Thomas Fumal for providing information about the geology of the Tarzana site; and Egill Hauksson for providing aftershock mechanisms. Leif Wennerberg, John Vidale, Robert Darraugh, T.-L. Teng, and an anonymous reviewer wrote excellent reviews that stimulated us to examine surficial geology more carefully. Any mention of commercial product names is for identification only and does not constitute an endorsement by the U.S. Geological Survey.

References

Andrews, D. J. (1986). Objective determination of source parameters and similarity of earthquakes of different sizes, in *Earthquake Source Mechanics,* Geophysical Monograph 37, American Geophysical Union, 259–267.

Bard, P.-Y. (1982). Diffracted waves and displacement field over two-dimensional elevated topographies, *Geophys. J. Int.* **71,** 731–760.

Boatwright, J., L. C. Seekins, T. E. Fumal, H.-P. Liu, and C. S. Mueller (1991). Ground motion amplification in the Marina District, *Bull. Seism. Soc. Am.* **81,** 1980–1997.

Boore, D. M., W. B. Joyner, and T. E. Fumal (1994). Estimation of response spectra and peak accelerations from Western North American earthquakes: an interim report, Part 2, *U.S. Geol. Surv. Open-File Rept. 94-127,* 40 pp.

Bonamassa, O. and J. E. Vidale (1991). Directional site resonances observed from aftershocks of the 18 October 1989 Loma Prieta earthquake, *Bull. Seism. Soc. Am.* **81,** 1945–1957.

Bonamassa, O., J. E. Vidale, H. Houston, and S. Y. Schwartz (1991). Directional site resonances and the influence of near-surface geology on ground motion, *Geophys. Res. Lett.* **18,** 901–904.

Bouchon, M. (1973). Effect of topography on surface motion, *Bull. Seism. Soc. Am.* **63,** 615–632.

Bouchon, M. and J. S. Barker (1995). Seismic response of a hill: the example of Tarzana, California, *Bull. Seism. Soc. Am.,* submitted.

Bouchon, M., C. A. Schultz, and M. N. Toksöz (1995). Effect of 3D topography on seismic motions, *J. Geophys. Res.,* submitted.

Çelebi, M. (1995). Northridge (California) earthquake: Unique ground motions, International Conference on Recent Advances in Geotechnical Earthquake Engineering and Soil Dynamics, April 2–7, 1995, St. Louis, Missouri, 6 pp.

Cormier, V. F. and P. Spudich (1984). Amplification of ground motion and waveform complexity in fault zones: examples from the San Andreas and Calaveras faults, *Geophys. J. R. Astr. Soc.* **79,** 135–152.

Dibblee, T. W. Jr. (1992). Geologic map of the Topanga and Canoga Park (South 1/2) Quadrangles, Los Angeles County, California, Map DF-35, Dibblee Geological Foundation, Santa Barbara, California.

Field, E. H. and K. H. Jacob (1995). A comparison and test of various site response estimation techniques, including three that are not reference-site dependent, *Bull. Seism. Soc. Am.* **85,** 1127–1143.

Fumal, T. E., J. F. Gibbs, and E. F. Roth (1981). In-site measurements of seismic velocity at 19 locations in the Los Angeles, California, region, *U.S. Geol. Surv. Open-File Rept. 81-399,* 121 pp.

Geli, L., P.-Y. Bard, and B. Jullien (1988). The effect of topography on earthquake ground motion: a review and new results, *Bull. Seism. Soc. Am.* **78,** 42–63.

Geosoils, Inc. (1992). Preliminary geotechnical investigation for Herman Properties, Work Order 3128-VN.

Hauksson, E., L. M. Jones, and K. Hutton (1995). The 1994 Northridge earthquake sequence in California: seismological and tectonic aspects, *J. Geophys. Res.* **100,** 12335–12355.

Hoots, H. W. (1931). Geology of the eastern part of the Santa Monica Mountains, Los Angeles County, California, *U.S. Geol. Surv. Profess. Pap. 165-C,* 134 pp.

Lee, W. H. K., R. A. White, D. H. Harlow, J. A. Rogers, P. Spudich, and D. A. Dodge (1994a). Digital seismograms of selected aftershocks of the Northridge earthquake recorded by a dense seismic array on February 10, 1994, at Cedar Hill Nursery in Tarzana, California, *U.S. Geol. Surv. Open-File Rept. 94-234,* 78 pp.

Lee, W. H. K., R. A. White, D. H. Harlow, J. A. Rogers, P. Spudich, and D. A. Dodge (1994b). Digital seismograms of selected aftershocks of the Northridge earthquake recorded by a dense seismic array on February 11, 1994, at Cedar Hill Nursery in Tarzana, California, *U.S. Geol. Surv. Open-File Rept. 94-234,* 78 pp.

Lee, W. H. K., R. A. White, D. H. Harlow, J. A. Rogers, P. Spudich, and D. A. Dodge (1994c). Digital seismograms of selected aftershocks of the Northridge earthquake recorded by a dense seismic array on February 12, 1994, at Cedar Hill Nursery in Tarzana, California, *U.S. Geol. Surv. Open-File Rept. 94-234,* 78 pp.

Li, Y.-G., J. E. Vidale, K. Aki, C. J. Marone, and W. H. K. Lee (1994). Fine structure of the Landers fault zone: segmentation and the rupture process, *Science* **265,** 367–370.

Shakal, A., M. Huang, and T. Cao (1988). The Whittier Narrows, California, earthquake of October 1, 1987: CSMIP strong motion data, *Earthquake Spectra* **4,** 75–100.

Shakal, A., M. Huang, R. Darragh, T. Cao, R. Sherburne, P. Malhotra, C. Cramer, R. Sydnor, V. Graizer, G. Maldonado, C. Peterson, and J. Wampole (1994). CSMIP Strong Motion Records from the Northridge, California, earthquake of 17 January 1994, Report OSMS 94-07, California Division of Mines and Geology, Sacramento, California.

Vidale, J. E. (1986). Complex polarization analysis of particle motion, *Bull. Seism. Soc. Am.* **76,** 1393–1405.

Vidale, J. E., O. Bonamassa, and H. Houston (1991). Directional site resonances observed from the 1 October 1987 Whittier Narrows, California, earthquake and the 4 October aftershock, *Earthquake Spectra* **7,** 107–125.

Wald, D. J. and T. H. Heaton (1994). A dislocation model of the 1994 Northridge, California, earthquake determined from strong ground motions, *U.S. Geol. Surv. Open-File Rept. 94-278,* 44 pp.

Wald, D. J., T. H. Heaton, and K. W. Hudnut (1996). The slip history of the 1994 Northridge, California, earthquake determined from strong motion, teleseismic, GPS, and leveling data, *Bull. Seism. Soc. Am.* **86,** no. 1B, S49–S70.

Wennerberg, L., R. D. Borcherdt, C. Mueller, C. Dietel, E. Sembera, R. Westerlund, and S. Hough (1994). Aftershock observations suggestive of large linear site amplification at the Cedar Hill Nursery accelerograph station, Tarzana, California, Abstracts with Program, Seismological Soc. of America Annual Meeting, Pasadena, California, April 5–7, 1994.

U.S. Geological Survey
345 Middlefield Road
Menlo Park, California 94025
E-mail: spudich@isdmnl.wr.usgs.gov

Manuscript received 11 January 1995.